

Electron momentum spectroscopy of NF_3 *

Li Jia-Ming(李嘉明), Miao Yu-Run(苗雨润), Deng Jing-Kang(邓景康), and Ning Chuan-Gang(宁传刚)[†]

Department of Physics, State Key Laboratory of Low-Dimensional Quantum Physics, Tsinghua University, Beijing 100084, China
Collaborative Innovation Center of Quantum Matter, Beijing 100084, China

(Received 18 March 2014; revised manuscript received 6 May 2014; published online 17 September 2014)

The electronic structure of nitrogen trifluoride was investigated by combining the high-resolution electron momentum spectroscopy with the high-level calculations. The experimental binding energy spectra and the momentum distributions of each orbital were compared with the results of Hartree–Fock, density functional theory (DFT), and symmetry-adapted-cluster configuration-interaction (SAC-CI) methods. SAC-CI and DFT-B3LYP with the aug-cc-pVTZ basis set can well reproduce the binding energy spectra and the observed momentum distributions of the valence orbitals except $1a_2$ and $4e$ orbitals. It was found that the calculated momentum distributions using DFT-B3LYP are even better than those using the high-level SAC-CI method.

Keywords: electron momentum spectroscopy, Dyson orbital, NF_3 , symmetry-adapted-cluster configuration-interaction (SAC-CI) method

PACS: 34.80.Gs, 31.15.V–

DOI: 10.1088/1674-1056/23/11/113403

1. Introduction

Nowadays, nitrogen trifluoride (NF_3) is predominantly used in the plasma etching and cleaning of semiconductors. The simple and symmetric structure makes NF_3 become one of the benchmark systems for many experimental and theoretical methods. The electronic structure of NF_3 has been previously investigated using photoelectron spectroscopy^[1] and electron energy-loss spectroscopy.^[2] Recently, the electron impact ionization and dissociation, and the dissociative electron attachment of NF_3 were reported.^[3–6] The electron momentum distribution of the highest occupied molecular orbital (HOMO) of NF_3 was reported by Brion *et al.*^[7] However, there is no detailed electron-momentum spectroscopy (EMS) result and theoretical explanations for the whole valence region of NF_3 . Especially, so far, no detailed interpretation of the ionization of NF_3 based on high-level many-body theories has been reported.

In the present work, we report the high resolution electron momentum spectroscopy of the whole valence orbitals of NF_3 . The high-level symmetry-adapted-cluster configuration-interaction (SAC-CI) method is employed to interpret the binding energy spectra and the electron momentum distributions. The theoretical results using the Hartree–Fock (HF) method and the density functional theory (DFT) are also presented for comparison.

2. Experimental and theoretical methods

Electron momentum spectroscopy is based on the kinetically complete ($e, 2e$) reaction.^[8–21] A bound electron of the

target molecule is knocked out by an impact electron, and the impact electron itself is scattered off. The energy E_0 and momentum p_0 of the incoming electron are predefined, and the energies and momenta of the two outgoing electrons can be precisely measured through the coincidental measurement. For the one-electron process, the binding energy ε of the bound electron is given by

$$\varepsilon = E_0 - E_1 - E_2, \quad (1)$$

where E_1 and E_2 are the energies of the two outgoing electrons. The spectrometer used in the present work takes the non-coplanar symmetric geometry.^[8–10] Under the high impact energy and the large momentum transfer, the binary-encountering approximation can be used. The magnitude of the momentum (p) of the bound electron before being struck out is obtained through measuring the relative azimuthal angle ϕ between the two outgoing electrons, i.e.,

$$p = \left\{ (2p_1 \cos \theta_1 - p_0)^2 + \left[2p_1 \sin \theta_1 \sin \left(\frac{\phi}{2} \right) \right]^2 \right\}^{1/2}, \quad (2)$$

where p_0 stands for the momentum of the incident electron, p_1 is the momentum of one of the two outgoing electrons ($p_1 = p_2$), and $\theta_1 = \theta_2 = 45^\circ$ are the polar angles of the outgoing electrons relative to the incident electron beam. Within the plane wave impulsive approximation (PWIA), the differential ($e, 2e$) cross section can be written as^[8–10]

$$\sigma_{\text{EMS}} \propto S_i^f \int d\Omega \left| \left\langle e^{-i\mathbf{p}\cdot\mathbf{r}} \Psi_f^{N-1} / \Psi_i^N \right\rangle \right|^2, \quad (3)$$

where S_i^f represents the spectroscopic factor, $e^{-i\mathbf{p}\cdot\mathbf{r}}$ stands for the plane wave, Ψ_i^N and Ψ_f^{N-1} are the wave functions of the ground state and the ionized state of the molecule,

*Project supported by the National Natural Science Foundation of China (Grant No. 11174175) and the Tsinghua University Initiative Scientific Research Program, China.

[†]Corresponding author. E-mail: ningcg@tsinghua.edu.cn

respectively, N is the total electron number of the neutral molecule, and $\int d\Omega$ represents the spherical average for the randomly oriented molecules in gas phase. The overlap integral $\langle \Psi_f^{N-1} | \Psi_i^N \rangle$ is called the Dyson orbital,^[12–25] which can be calculated using high-level many-body computational methods, such as the configuration interaction method and Green's function theory. With the frozen orbital approximation, the Dyson orbital can be simplified as a Hartree–Fock orbital or a Kohn–Sham orbital,^[24,25] i.e.,

$$\sigma_{\text{EMS}} \propto S_i^f \int d\Omega |\varphi_j(p)|^2, \quad (4)$$

where $\varphi_j(p)$ is the j -th Hartree–Fock or Kohn–Sham orbital in the momentum space.

In the present experiment, the instrumental energy resolution is 0.7 eV (full width at half maximum, FWHM), which is obtained through the calibration experiment of an Ar sample. The finite acceptance angle of θ is $\pm 0.84^\circ$ (one standard error), and the resolution of azimuthal angle ϕ is $\pm 0.53^\circ$ (one standard error).^[26,27] The gas sample NF_3 with a purity of 99.9% is used directly. No impurities are evidently observed in the binding energy spectra. To check the PWIA, the experiment is conducted at the impact energies of 1200 eV and 600 eV.

The SAC-CI method, which was developed by Nakatsuji and his co-workers,^[28–30] was recently introduced for interpreting the electron momentum spectroscopy by our group.^[31–34] There are two options, SD- R and general- R , in SAC-CI calculations. In the SAC-CI general- R method, quadruple or even higher excitation operators R can be chosen to include the higher-order electron correlation, which is necessary for interpreting the ionization of the inner valence orbitals. The SAC-CI combines the merits of the size consistency of the cluster expansion and the energy upper boundary of the CI. In the present work, the SAC-CI general- R method with the correlation consistent basis set cc-pVDZ^[35] is used for interpreting the electron binding energy spectra of NF_3 . The active space includes all HF reference orbitals except the four core orbitals (one N_{1s} , three F_{1s}). The excitation operators R up to quadruples are included. Perturbation selections are done to reduce the computational cost. The threshold of the linked terms for the ground state is 1.0×10^{-6} , and the unlinked terms are included as the products of the linked terms whose single- and double-configuration-interaction (SDCI) coefficients are greater than 5.0×10^{-6} . In total, 500 final states are calculated for reproducing the experimental binding energy spectrum. The SAC-CI calculations with the more complete basis sets cc-pVTZ and aug-cc-pVTZ^[28] are also conducted for better describing the experimental momentum distributions. Only the Dyson orbitals in the outer valence region are constructed using aug-cc-pVTZ due to the very high computational cost.

The SAC-CI, HF, and DFT calculations are conducted with G03 program.^[36] In the present work, aug-cc-pVTZ is used as the default basis set if not explicit specification elsewhere. Fourier transformations and the spherical average of the momentum distributions for the molecular orbitals are calculated with our home-compiled NEMS program.^[37]

3. Results and discussion

3.1. Binding energy spectra of NF_3

The geometry structure of NF_3 is shown in the inset of Fig. 1(b). It has the C_{3v} symmetry at equilibrium. The electronic configuration of the ground state can be written as

$$(\text{core})^8 \underbrace{(1a_1)^2 (1e)^4 (2a_1)^2 (2e)^4 (3a_1)^2 (3e)^4 (4e)^4}_{\text{inner valence}} \underbrace{(1a_2)^2 (4a_1)^2}_{\text{outer valence}}.$$

The $4a_1$ is the highest occupied molecular orbital. The binding energy spectra of NF_3 in the region of 9–53 eV are shown in Fig. 1. To obtain the experimental momentum distribution for each orbital, the experimental binding energy spectrum at each azimuthal angle is fitted by twelve Gaussian functions. The widths of the Gaussian functions have considered the spectrometer energy resolution and the Frank–Condon widths estimated from the photoelectron spectra.^[1] Figure 1(b) shows

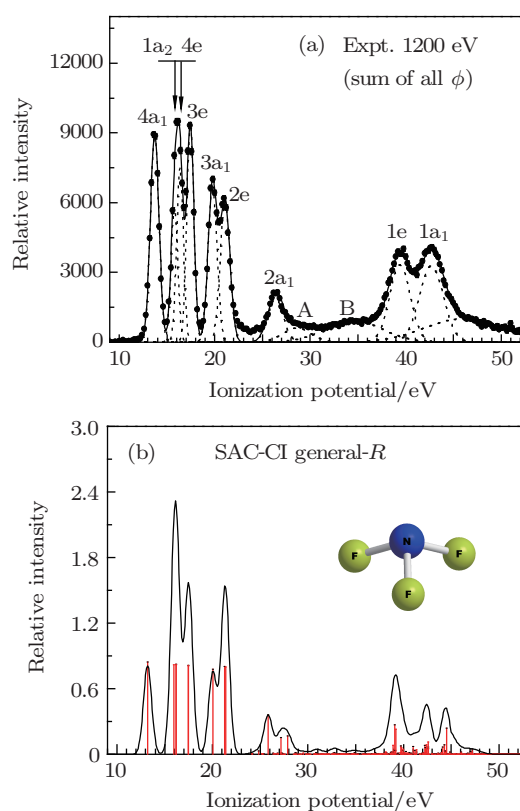


Fig. 1. (color online) Binding energy spectra of NF_3 . (a) (e, 2e) ionization spectra summed over all ϕ angles obtained at impact energy of 1200 eV plus binding energies. The dashed line represent the individual fitting Gaussian peak and the solid line is their summation. (b) Simulated ionization spectrum using the SAC-CI general- R method with cc-pVDZ basis set. The heights of the sticks under the curve represent the spectroscopic factors. The inset is the molecular structure of NF_3 .

the simulated ionization spectrum using the SAC-CI general-*R* method with the cc-pVDZ basis set. The vertical bars under the curve represent the spectroscopic factors for each Dyson orbital. In general, the simulation is in excellent agreement with the experimental binding energy spectrum.

In the outer valence regions (< 22 eV), each Dyson orbital has one dominant HF orbital component. The main lines at 13.71 eV, 15.77 eV, 16.36 eV, 17.45 eV, 19.77 eV, and 21.09 eV can be considered as the ionization from $4a_1$, $1a_2$, $4e$, $3e$, $3a_1$, and $2e$ orbitals, respectively. The origin of the intensity at around 23.5 eV in Fig. 1(a) is not clear. It may be due to some higher-order excitations or dissociation–excitation processes, which have not been included in the SAC-CI/cc-pVDZ calculation. As Fig. 1 shows, in the region of 25–30 eV, the $2a_1$ orbital mainly split into three satellite lines according to the prediction of the SAC-CI calculation. In the region of 30–38 eV, a broad band labeled as band B is observed. SAC-CI/cc-pVDZ predicts more than 100 weak lines in this region, and their summed spectroscopic factor is only 0.3. In the region of 38–50 eV, two resolvable features are observed, which are the results of ionization from $1e$ and $1a_1$ orbitals, respectively. The experimental spectra do not have the pre-

dicted additional splitting at 27 eV and 44 eV, which might be due to some broadening effects which are not considered in the calculations. The experimental ionization potentials and spectroscopic factors of these peaks and the calculated values are compared in details in Table 1. The ionization potentials in the outer valence region predicted using the SAC-CI general-*R* method with cc-pVTZ and aug-cc-pVTZ basis sets are also listed for comparison. As can be seen, the differences among the predicted ionization potentials by SAC-CI with different basis sets are very small. For example, the predicted ionization potential of the HOMO is 13.20 eV by cc-pVDZ, 13.24 eV by cc-pVTZ, and 13.55 eV by aug-cc-pVTZ, which are very close to the experimental value 13.71 eV. This indicates that cc-pVDZ is good enough for interpreting the experimental binding energy spectra. However, as shown later, cc-pVDZ is too limited to describe the experimental momentum distributions. In Table 1, the shifted B3LYP method also predicts very accurate ionization potentials. Here, the shift B3LYP means a global shift of the negatives of the orbital energies obtained with the B3LYP/aug-cc-pVTZ method to align the HOMO with the first experimental peak.

Table 1. Ionization potentials (eV) and spectroscopic factors (in parentheses) of NF_3 .

	EMS ^{a)}	PES ^{b)}	SAC-CI ^{c)}			Shifted B3LYP ^{d)}
			cc-pVDZ	cc-pVTZ	aug-cc-pVTZ	
$4a_1$	13.71 (0.82)	13.71	13.20 (0.84)	13.24 (0.84)	13.55 (0.85)	13.71
$1a_2$	15.77 (0.82)	15.81	15.98 (0.83)	16.04 (0.83)	16.27 (0.84)	15.89
$4e$	16.36 (0.82)	16.32	16.18 (0.83)	16.27 (0.83)	16.48 (0.84)	16.31
$3e$	17.45 (0.82)	17.44	17.50 (0.82)	17.49 (0.82)	17.81 (0.83)	17.53
$3a_1$	19.77 (0.82)	19.74	20.02 (0.79)	20.03 (0.80)	20.37 (0.81)	20.00
$2e$	21.09 (0.82)	21.09	21.33 (0.81)	21.20 (0.82)	21.55 (0.84)	21.35
$2a_1$	26.37 (0.82)	26.37	25.82 (0.36)			26.54
		28.6 (0.25)	27.16 (0.15)			
			27.89 (0.17)			
B	34.6 (0.81)		34–38 (0.30)			
$1e$	39.4 (0.37)		38.94 (0.08)			38.03
			39.09 (0.27)			
			39.23 (0.23)			
			39.74 (0.08)			
			39.80 (0.06)			
			39.98 (0.05)			
			41.02 (0.07)			
			41.39 (0.04)			
$1a_1$	42.7 (0.27)		42.26 (0.08)			41.59
			42.31 (0.06)			
			42.40 (0.09)			
			42.59 (0.05)			
			42.60 (0.07)			
			42.61 (0.11)			
			44.12 (0.07)			
			44.32 (0.09)			
			44.55 (0.24)			
			47.24 (0.04)			

^{a)} Present work. The ionization energies determined by the high resolution PES are directly used as the initial values in fitting EMS binding energy spectra, and then a slight adjustment is made for best fitting the experimental spectra.

^{b)} Ref. [1].

^{c)} Only the ionization potentials for the outer valence orbitals are calculated due to the extremely high computational cost with cc-pVTZ and aug-cc-pVTZ basis sets. Only those Dyson orbitals with spectroscopic factors greater than 0.04 are listed here.

^{d)} The negatives of the orbital energies are shifted to align the ionization from $4a_1$ orbital (HOMO) with the first experimental peak.

3.2. Momentum distributions of NF_3

The experimental momentum distributions of the HOMO are compared with the theoretical calculations using various methods in Fig. 2. Since the experimental intensity is in a relative scale, a normalization procedure is needed to rescale the experimental momentum distributions. Here we compare the summed experimental momentum distributions of all outer valence orbitals with those of the summed B3LYP calculations to determine the global normalization constant (see Fig. 3). The global constant is directly used to normalize the experimental momentum distributions of the outer valence orbitals, and to determine the experimental spectroscopic factors of the inner valence orbitals. The averaged pole strength 0.82 of the outer-valence orbitals predicted by SAC-CI/cc-pVDZ is uniformly assigned as the pole strength of the outer-valence orbitals. The experimental momentum distributions of the HOMO in Fig. 2 agree with those reported by Brion *et al.*^[7] It can be seen that HF, B3LYP, and SAC-CI methods with aug-cc-pVTZ (curves 1, 2, 5) can well reproduce the experimental momentum distributions. However, SAC-CI with cc-pVDZ and cc-pVTZ calculations significantly underestimate the experimental intensity in the low momentum region although their predictions for the ionization potentials are quite accurate. The reason for the phenomenon is that the intensity in the low momentum region is mainly contributed from the diffuse part of the molecular orbitals, which are usually far away from the nuclei in real space according to the Fourier transform theorem. Aug-cc-pVTZ includes more diffuse and polar basis functions than cc-pVDZ and cc-pVTZ. The diffuse part usually contributes much less to the total energy of the molecule than the part near the nuclei, but it is important to describe the momentum distribution in the low momentum region. It should be noted that the HOMO of NF_3 is not a classic N_{2p} lone pair orbital as generally believed. With the B3LYP/aug-cc-pVTZ method, the Mulliken population analysis indicates that the HOMO is composed of 49% F_{2p} , 28% N_{2p} , and 21% N_{2s} . There is a notable intensity distributed between N atom and F atoms. As a contrast, $1a_2$, $4e$, and $3e$ are dominantly composed of F_{2p} electrons (see Fig. 4). Their binding energies are very close. The momentum distributions of these orbitals are shown in Fig. 5.

In Fig. 5(a), HF, B3LYP, and SAC-CI predict almost the same momentum distributions for the $1a_2$ orbital. They all significantly underestimate the experimental intensity in the low momentum region. In Fig. 5(b), the three methods can roughly reproduce the experimental profiles of the $4e$ orbital, however there is a notable discrepancy around $p = 1.5$ a.u. By considering that the two ionized states overlap significantly (see Fig. 1), the summed momentum distributions of $1a_2$ and $4e$ orbitals are plotted in Fig. 5(c). However, the discrepancies still exist in the low momentum region. Therefore, the discrepancies are not likely due to the overlap of the two orbitals.

The discrepancies may be due to the distorted wave effects, which have been observed before.^[38–41] There is a perceptible difference between the experimental momentum distributions at 1200 eV and those at 600 eV, which partly confirms the explanation. To check the possibility of nuclear dynamics^[42,43] and the Jahn–Teller distortion on the momentum distributions, some approximated calculations have been conducted according to the methods by Watanabe *et al.*^[44] and our work on

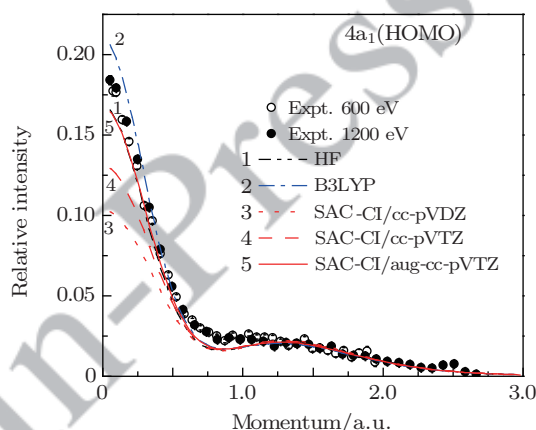


Fig. 2. (color online) Spherically averaged momentum distributions of the HOMO of NF_3 . The instrumental resolution has been convoluted in the theoretical calculations.

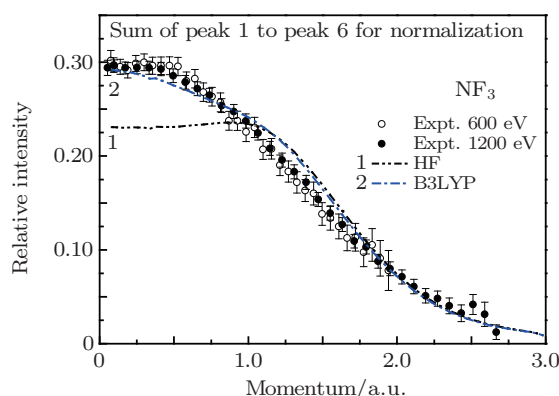


Fig. 3. Normalization of experimental momentum distributions of NF_3 .

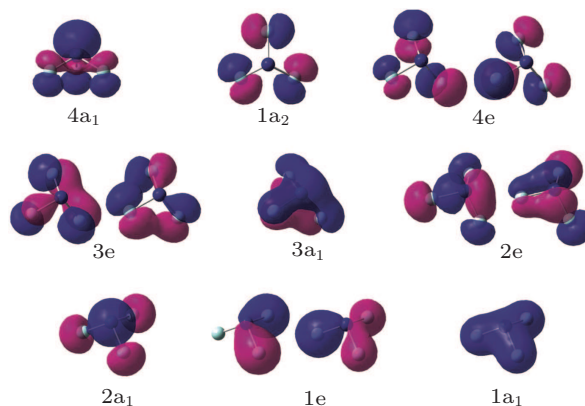


Fig. 4. (color online) Molecular orbitals of NF_3 .

NH_3 .^[45] No evident effect on the momentum distributions is found. In Fig. 5(d), the HF method cannot well describe the experimental momentum distribution of the 3e orbital in the

low momentum region, and SAC-CI improves. Unexpectedly, the B3LYP method best reproduces the experimental distributions.

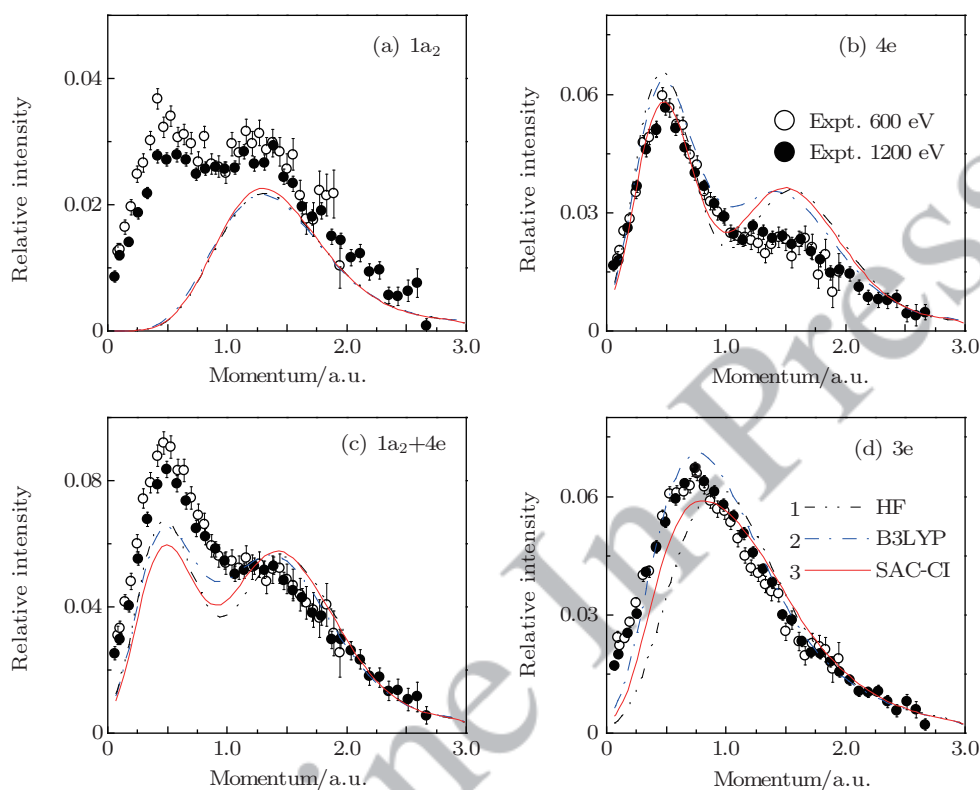


Fig. 5. (color online) Spherically averaged momentum distributions of (a) $1a_2$, (b) $4e$, (c) $1a_2+4e$, and (d) $3e$ orbitals of NF_3 .

The similar situations are also observed for $3a_1$ and $2e$ orbitals in Fig. 6. The prediction of the B3LYP method fits with the experimental distributions of the $3a_1$ orbital perfectly. The HF method significantly underestimates the experimental intensity in the low momentum region. The SAC-CI/aug-cc-pVTZ method can describe the overall profiles of the experimental distributions. However, the details of the predicted shape are different from those of the experimental distributions in the low momentum region. The calculated momentum distributions using the SAC-CI method with smaller basis sets cc-pVDZ and cc-pVTZ are also plotted for comparison. Again, we see that SAC-CI with the two smaller basis sets cannot reproduce the experimental momentum distributions of $3a_1$ although they predict accurate ionization potentials for the $3a_1$ orbital. For the $2e$ orbital, the calculated momentum distributions by HF and SAC-CI are narrower than the experimental distribution, and the calculated maximum intensity is higher than the observed one. The agreement between the theoretical distributions using the B3LYP method and the experimental distributions is much better. It can be seen that the discrepancies between experimental and theoretical distributions are more remarkable in the low momentum region. There are two reasons. One is that our spectrometer is more sensitive for the

small angle scattering, and the other is that the intensity in the high momentum region decreases as p^{-4} . Recently, we observed similar effects in the highly symmetric molecules, such as CX_4 ($X = \text{F}, \text{Cl}, \text{Br}$).^[46]

In the inner valence region, the $2a_1$ orbital mainly splits into three lines located at 25.82 eV, 27.16 eV, and 27.89 eV, respectively, according to the SAC-CI predictions. Two Gaussian functions ($2a_1$ and A) are used to extract their experimental momentum distributions. In Figs. 7(a) and 7(b), the experimental momentum distributions are compared with HF and B3LYP theoretical results. Apparently, HF significantly underestimates the experimental intensity in the low momentum region, and B3LYP can describe the overall profiles of the experimental distributions. However, there are notable discrepancies in the low momentum region in Figs. 7(a) and 7(b). The discrepancies decrease as the impact energy increases from 600 eV to 1200 eV. It might be due to the distorted wave effect.^[34-37] To interpret the experimental momentum distributions of band B, all satellite lines between 30 eV and 38 eV predicted by SAC-CI/cc-pVDZ are summed up. The calculated intensity is much lower than the experimental intensity. However, the calculated momentum distribution agrees with the experimental one well if multiplying it by 2.7. The

summed spectroscopic factor predicted by SAC-CI/cc-pVDZ is 0.30, so the experimental spectroscopic factor is estimated as 0.81. The experimental momentum distributions of $1e$ and $1a_1$ orbitals are shown in Figs. 7(d) and 7(e), which can be described by B3LYP and HF methods. In contrast to the remarkable difference between the momentum distributions for other orbitals obtained by HF and B3LYP, there are no differences between the two methods for $1e$ and $1a_1$ orbitals. These

two orbitals are mainly composed of F_{2s} and N_{2s} electrons. The deviations of the theoretical profiles from the experimental momentum distributions in the high momentum region are mainly due to the congested satellite lines in the inner valence region, and the inner valence orbitals are closer to the nuclei, thus the incoming and the out-going electrons represented by the plane waves are influenced more by the nuclear potential.

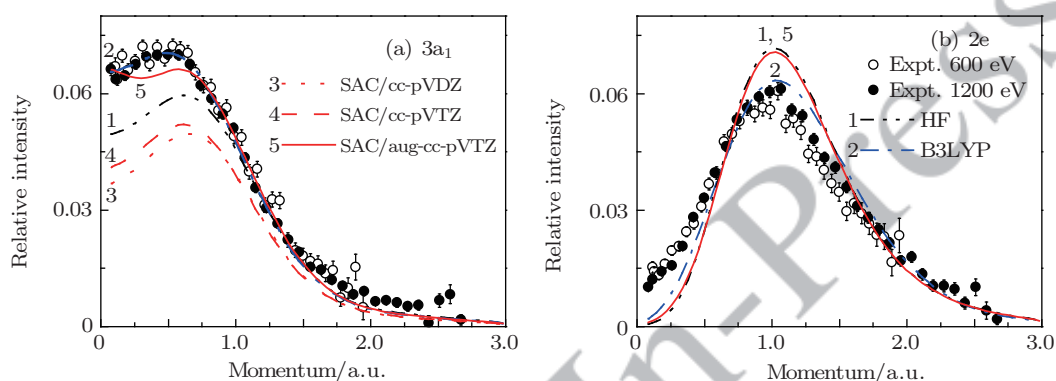


Fig. 6. (color online) Spherically averaged momentum distributions of (a) $3a_1$ and (b) $2e$ orbitals of NF_3 .

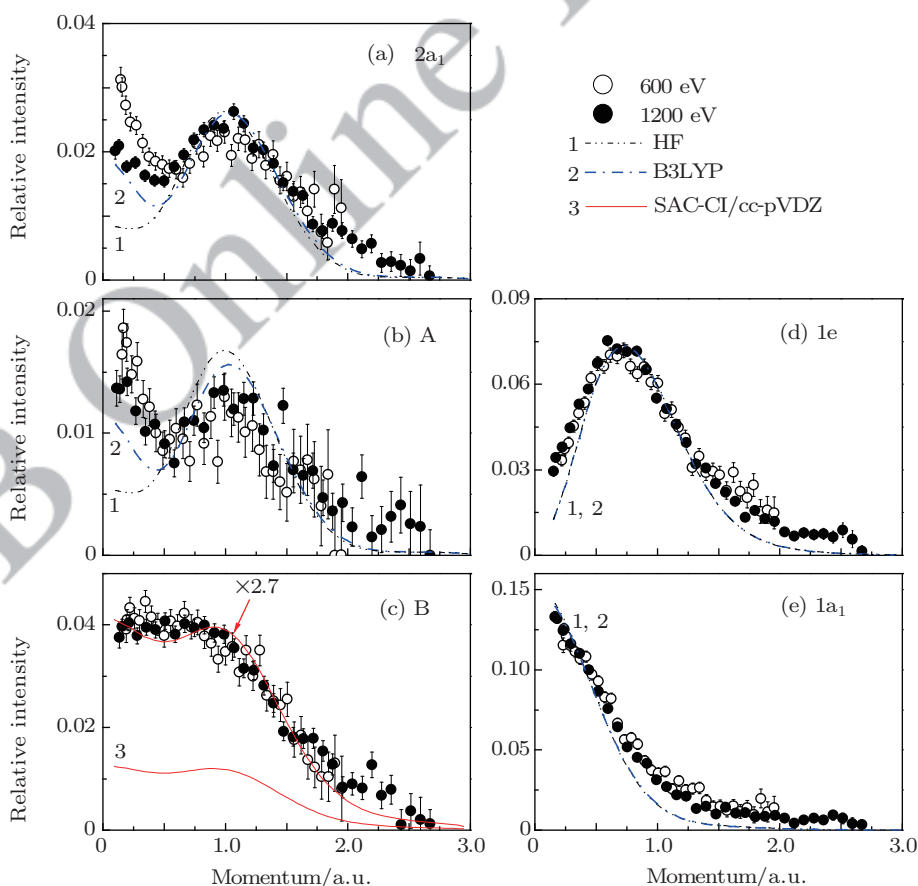


Fig. 7. (color online) Spherically averaged momentum distributions of (a) $2a_1$ orbital, (b) A and (c) B bands, (d) $1e$ and (e) $1a_1$ orbitals of NF_3 .

It is interesting to note that the B3LYP method can predict very accurate the ionization potentials with a simple shift and describe the experimental momentum distributions even

better than the high-level SAC-CI method. It may be due to some error cancellation. For example, most of the currently used exchange–correlation potentials have asymptotic

errors.^[47] Such an error cancellation is unusual since it cancels the calculation errors for the ionization potentials and the electron momentum distributions simultaneously.

4. Summary

The electronic structure of NF_3 was extensively studied by electron momentum spectroscopy in combination with the high-level calculations. The SAC-CI method can well reproduce the experimental binding energy spectra in the range of 10–50 eV. The calculated momentum distributions using the SAC-CI/aug-cc-pVTZ method agree well with the experimental results for most molecular orbitals of NF_3 except the $1a_2$ and $4e$ orbitals. It was found that the calculated ionization potentials using the DFT-B3YP method with a simple shift fit with the experimental binding energies very well and the predicted electron momentum distributions using the DFT-B3LYP method are even better than that using the high-level SAC-CI method.

References

- [1] Jörgensen A and Cavell R G 2003 *J. Electron Spectrosc. Relat. Phenom.* **128** 245
- [2] Sodhi R N S, Brion C E and Cavell R G 1984 *J. Electron Spectrosc. Relat. Phenom.* **33** 4
- [3] Xia X L, Zeng X J, Li H K, Wu B and Tian S X 2013 *Angew. Chem. Int. Ed.* **52** 1013
- [4] Szmytkowski C, Domaracka A, Mozejko P, Ptasńska-Denga E, Kłosowski Ł, Piotrowicz M and Kasperski G 2004 *Phys. Rev. A* **70** 032707
- [5] Li H K, Xia L, Zeng X J and Tian S X 2013 *J. Phys. Chem. A* **117** 3176
- [6] Aschi M and Grandinetti F 2000 *J. Mol. Struct.* **497** 205
- [7] Bawagan A O and Brion C E 1987 *Chem. Phys. Lett.* **137** 573
- [8] McCarthy I E and Weigold E 1991 *Rep. Prog. Phys.* **54** 789
- [9] Coplan M A, Moore J H and Doering J P 1994 *Rev. Mod. Phys.* **66** 985
- [10] Weigold E and McCarthy I E 1999 *Electron Momentum Spectroscopy* (New York: Kluwer Academic/Plenum Publishers)
- [11] Liu K, Deng J K and Ning C G 2010 *Chin. Phys. Lett.* **27** 073403
- [12] Fan L L, Zhong Z P, Zhu L F, Liu X J, Cheng H D, Yuan Z S and Xu K Z 2005 *Chin. Phys. B* **14** 2478
- [13] Lin M, Liu Y W, Zhong Z P and Zhu L F 2013 *Chin. Phys. B* **22** 023404
- [14] Shi L L, Liu K, Luo Z H, Ning C G and Deng J K 2011 *Chin. Phys. B* **20** 113403
- [15] Zhang Z, Shan X, Wang T, Wang E and Chen X J 2014 *Phys. Rev. Lett.* **112** 023204
- [16] Xu S Y, Ma X W and Ren, X G, Senftleben A, Pfluger T, Yan S C, Zhang P J, Yang J, Ullrich J and Dorn A 2013 *J. Chem. Phys.* **138** 134307
- [17] Guo D L, Ma X W, Ren X G, Senftleben A, Pfluger T, Yan S C, Zhang P J, Yang J, Ullrich J and Dorn A 2011 *Acta Phys. Sin.* **60** 113401 (in Chinese)
- [18] Yang T C, Ren X G, Ning C G, Su G L, Deng J K, Zhang S F, Ren X G and Huang Y R 2006 *Chin. Phys. Lett.* **23** 1157
- [19] Zhang S F, Ning C G, Huang Y R, Liu K and Deng J K 2009 *Acta Phys. Sin.* **58** 2382 (in Chinese)
- [20] Xu C K, Chen X J, Jia C C, Zhang X H, Yin X F, Shan X, Wei Z and Xu K Z 2002 *Chin. Phys. Lett.* **19** 1795
- [21] Liu K, Ning C G and Deng J K 2010 *Chin. Phys. Lett.* **27** 073403
- [22] Singh R K, Ortiz J V and Mishra M K 2010 *Int. J. Quantum Chem.* **110** 1901
- [23] Oana C M and Krylov A I 2007 *J. Chem. Phys.* **127** 234106
- [24] Duffy P, Chong D P, Casida M E and Salahub D R 1994 *Phys. Rev. A* **50** 4707
- [25] Zheng Y, Brion C E, Brunger M J, Zhao K, Grisogono A M, Braidwood S, Weigold E, Chakravorty S J, Davidson E R, Sgamellotti A and Niessen W V 1996 *Chem. Phys.* **212** 269
- [26] Ning C G, Zhang S F, Deng J K, Liu K, Huang Y R and Luo Z H 2008 *Chin. Phys. B* **17** 1729
- [27] Ren X G, Ning C G, Deng J K, Zhang S F, Su G L, Huang F and Li G Q 2005 *Rev. Sci. Instrum.* **76** 063103
- [28] Nakatsuji H 1978 *Chem. Phys. Lett.* **59** 362
- [29] Nakatsuji H 1979 *Chem. Phys. Lett.* **67** 329
- [30] Nakatsuji H and Hirao K 1981 *Int. J. Quantum Chem.* **20** 1301
- [31] Miao Y R, Ning C G and Deng J K 2011 *Phys. Rev. A* **83** 062706
- [32] Miao Y R, Ning C G, Liu K and Deng J K 2011 *J. Chem. Phys.* **134** 204304
- [33] Zhu J S, Deng J K and Ning C G 2012 *Phys. Rev. A* **85** 052714
- [34] Miao Y R, Deng J K and Ning C G 2012 *J. Chem. Phys.* **136** 124302
- [35] Dunning T H 1989 *J. Chem. Phys.* **90** 1007
- [36] Frisch M J, Trucks G W, Schlegel H B, et al. 2004 *GAUSSIAN 03*, Revision E.01 (Gaussian Inc., Wallingford, CT)
- [37] Ning C G, Hajgató B, Huang Y R, Zhang S F, Liu K, Luo Z H, Knippenberg S, Deng J K and Deleuze S 2008 *Chem. Phys.* **343** 19
- [38] Brion C E, Zheng Y, Rolke J, Neville J J, McCarthy I E and Wang J 1998 *J. Phys. B* **31** L223
- [39] Takahashi M, Saito T, Hiraka J and Udagawa Y 2003 *J. Phys. B* **36** 2539
- [40] Ren X G, Ning C G, Deng J K, Zhang S F, Su G L, Huang F and Li G Q 2005 *Phys. Rev. Lett.* **94** 163201
- [41] Ning C G, Ren X G, Deng J K, Su G L, Zhang S F and Li G Q 2006 *Phys. Rev. A* **73** 022704
- [42] Hajgató B, Deleuze M S and Morini F 2009 *J. Phys. Chem. A* **113** 7138
- [43] Shojaei S H, Vandenbussche J, Deleuze M S and Bultinck P 2013 *J. Phys. Chem. A* **117** 8388
- [44] Watanabe N, Yamazaki M and Takahashi M 2012 *J. Chem. Phys.* **137** 114301
- [45] Zhu J S, Miao Y R, Deng J K and Ning C G 2012 *J. Chem. Phys.* **137** 174305
- [46] Ning C G, Zhu J S, Deng J K and Miao Y R 2014 *J. Phys.: Conf. Ser.* **488** 052027
- [47] Casida M E, Jamorski C, Casida K C and Salahub D R 1998 *J. Chem. Phys.* **108** 4439